JACS
JOURNAL OF THE AMERICAN CHEMICAL SOCIETY

Article

Titanium(III)-Oxo Clusters in a Metal-Organic Framework Support Single-Site Co(II)-Hydride Catalysts for Arene Hydrogenation

Pengfei Ji, Yang Song, Tasha Drake, Samuel S. Veroneau, Zekai Lin, Xiandao Pan, and Wenbin Lin

J. Am. Chem. Soc., **Just Accepted Manuscript** • DOI: 10.1021/jacs.7b11241 • Publication Date (Web): 06 Dec 2017

Titanium(III)-Oxo Clusters in a Metal-Organic Framework Support Single-Site Co(II)-Hydride Catalysts for Arene Hydrogenation

Pengfei Ji,[a] Yang Song,[a] Tasha Drake,[a] Samuel S. Veroneau,[a] Zekai Lin,[a] Xiandao Pan[b,*] and Wenbin Lin[a,*]

[a]Department of Chemistry, University of Chicago, 929 E 57th St, Chicago, IL 60637, USA

[b]State Key Laboratory of Bioactive Substances and Functions of Natural Medicines, Institute of Materia Medica, Chinese Academy of Medical Sciences & Peking Union Medical College, Beijing 100050, China

ABSTRACT: Titania (TiO_2) is widely used in the chemical industry as an efficacious catalyst support, benefiting from its unique strong metal-support interaction. Many proposals have been made to rationalize this effect at the macroscopic level, yet the underlying molecular mechanism is not understood due to the presence of multiple catalytic species on TiO_2 surface. This challenge can be addressed with metal-organic frameworks featuring well-defined metal oxo/hydroxo clusters for supporting single-site catalysts. Herein we report that the $Ti_8(\mu_2\text{-}O)_8(\mu_2\text{-}OH)_4$ node of the Ti-BDC MOF (MIL-125) provides a single-site model of the classical TiO_2 support to enable Co^{II}-hydride catalyzed arene hydrogenation. The catalytic activity of the supported Co^{II}-hydride is strongly dependent on the reduction of the Ti-oxo cluster, definitively proving the pivotal role of Ti^{III} in the performance of the supported catalyst. This work thus provides a molecularly precise model of Ti-oxo clusters for understating the strong metal-support interaction of TiO_2-supported heterogeneous catalysts.

Introduction

Metal oxides have found broad applications in the chemical industry as catalyst supports by using surface oxo/hydroxo groups to coordinate to catalytic metal centers. Such surface oxo/hydroxo ligands are readily available, thermally robust, and chemically stable, but lack tunability of their electronic and steric properties when compared to organic ligands that are used to support homogeneous catalysts. In this context, TiO_2 is one of the most efficacious metal oxide catalyst supports, due to its negligible toxicity, low price, high stability, and most interestingly, tunable electronic property through the titanium redox activity.[1-2] Previous research into TiO_2-supported catalysts has uncovered the strong metal-support interaction (SMSI) effect, which occurs when metallic or metal oxide catalysts are immobilized on TiO_2 followed by thermal treatment.[3-5] The SMSI effect has been shown to significantly impact catalytic activity and selectivity. Although many proposals have been put forth to explain this effect at the macroscopic level, including TiO_2 migration,[6] local Ti^{IV} reduction to Ti^{III},[5, 7] substrate activation with the surface O-vacancies,[8-9] there is still not a clear understanding of the SMSI effect at the molecular level. The difficulty in understanding the effects of metal oxide supports partly arises from the presence of multiple species, due to the catalyst binding to different crystal faces, different binding modes within one certain crystal face, and pervasive defects at the molecular level (Figure 1a).[10-12] Thus, it is highly desirable to design structurally defined Ti-oxo surfaces to support single-site catalytic metal centers in order to precisely pinpoint the effects of the Ti-oxo support on catalytic activity and selectivity.

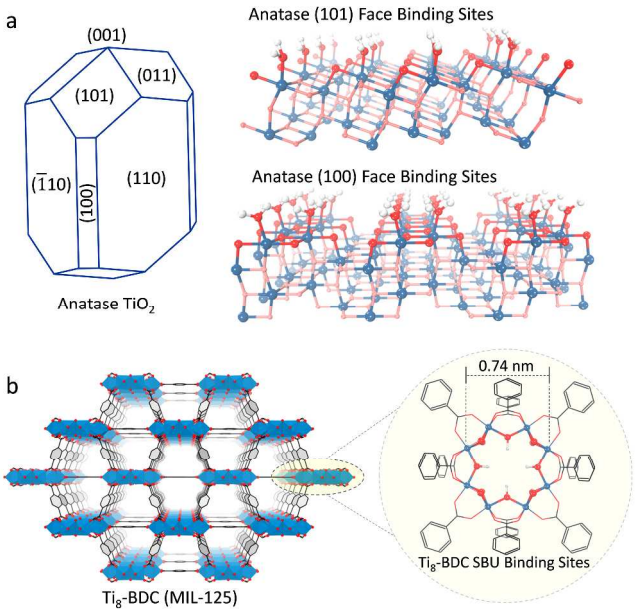

Figure 1. (a) Schematic representation of possible faces on the anatase phase of TiO_2 (left) and surface structures of the (101) face (top right) and (100) face (bottom right). The first layer of oxygen atoms on each of the faces are highlighted in red. All of these faces can undergo surface metalation leading to multiple catalytic sites. (b) Ti_8 SBUs in the Ti_8-BDC MOF have one possible binding site only and support the formation of single-site catalysts.

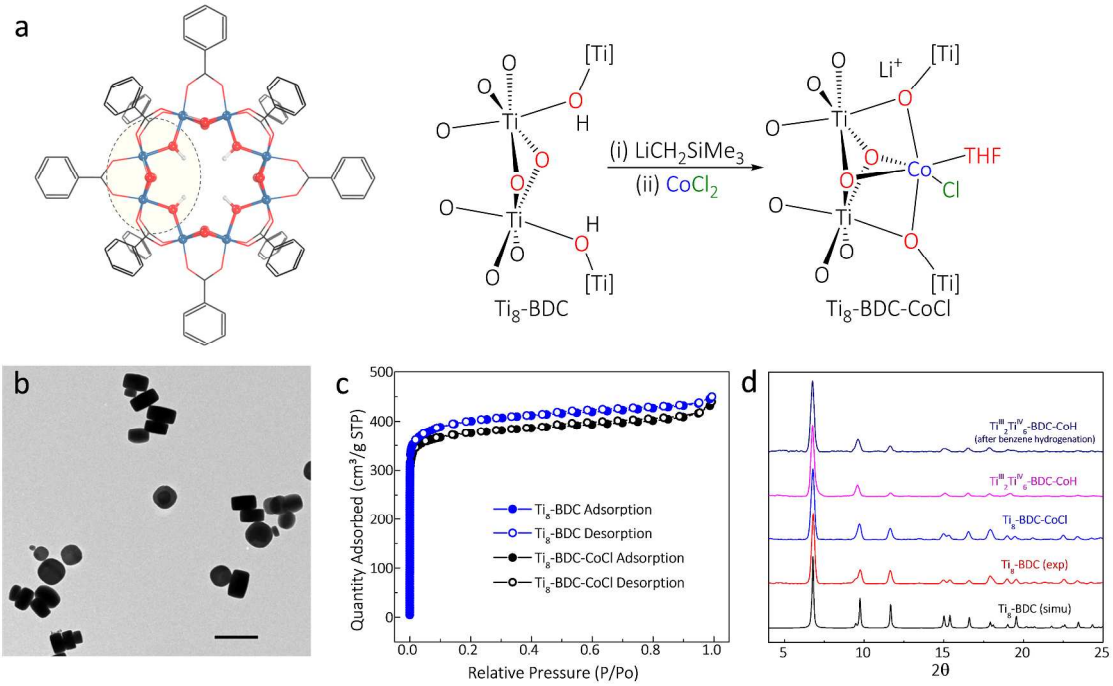

Figure 2. (a) Depiction of the tetradentate binding pocket of the Ti_8 node and the cobalt coordination environment within the binding pocket. (b) TEM image of Ti_8-BDC-CoCl, showing the same morphology as pristine Ti_8-BDC. The scale bar is 1 μm. (c) Nitrogen sorption isotherms of Ti_8-BDC and Ti_8-BDC-CoCl. The BET surface area of Ti_8-BDC-CoCl (1479 m^2/g) is slightly lower than that of Ti_8-BDC (1552 m^2/g) due to the increase of molecular weight after metalation. (d) The similarity of PXRD patterns of Ti_8-BDC (red), Ti_8-BDC-CoCl (blue), Ti_8-BDC-CoH (pink), and Ti_8-BDC-CoH recovered from benzene hydrogenation (navy) to the simulated PXRD pattern for Ti_8-BDC (black) indicates that the crystallinity of the MOF was maintained after metalation, reduction, and catalysis.

Over the past two decades, metal-organic frameworks (MOFs) have emerged as a highly tunable platform for the design of single-site solid catalysts.[13-15] Compared to traditional *heterogeneous* metal oxide-based catalysts, porous MOF catalysts allow uniform functionalization of the interior channels and pores to afford more efficient single-site solid catalysts. MOFs share a similarity to industrially important zeolite catalysts that are characterized by large internal surface areas and uniform pore sizes,[16] but can be constructed from a variety of organic linkers and inorganic nodes to afford an infinite array of structurally defined single-site solid catalysts. For example, many types of MOF catalysts have been prepared through channel entrapment,[17-19] organic linker functionalization,[20] and, most recently, inorganic node functionalization.[21-24] In particular, MOF nodes with oxo/hydroxo functionalities have recently been used to support earth-abundant metals to generate highly active metal oxide-supported catalysts for a range of organic transformations. MOF node supported catalysts are truly single-site and tunable, promising a unique approach to systematic investigation of the electronic and steric effects of metal-oxo supports on catalytic performances.

In this work, we used Ti-oxo/hydroxo secondary building unit (SBU) of the titanium-based MOF, MIL-125 (Ti_8-BDC, BDC is 1,4-benzenedicarboxylate),[25] to support Co^{II}-H catalysts for highly effective arene hydrogenation (Figure 1b). Ti_8-BDC features a nano-sized octa-titanium cluster with structurally defined bridging hydroxides and oxides, serving as an excellent molecular model to study the electronic effects of TiO_2 on the catalytic performance of supported catalysts. We observed Co-mediated dihydride reductive elimination to form H_2 and the spillover of electrons to reduce Ti^{IV} to Ti^{III} on Ti-oxo SBUs.[26] The reduction of Ti-oxo SBUs tuned the electronic properties of Co^{II}-H catalysts to effect the hydrogenation of arenes and heteroarenes with exceptional activities.

Results and Discussion

Structure and Co Binding Mode of Ti_8-BDC-CoCl. The Ti_8-BDC MOF, with the formula of $Ti_8O_8(OH)_4(BDC)_6$, was prepared solvothermally from $Ti(O^iPr)_4$, H_2BDC, methanol, and dimethylformamide (DMF) according to the literature procedure.[25] Ti_8-BDC was first deprotonated with $LiCH_2SiMe_3$ to generate a $Ti_8O_8(OLi)_4(BDC)_6$ intermediate, and then metalated with 1 equiv. of $CoCl_2$ to generate Ti_8-BDC-CoCl as a turquoise solid (Figure 2a). The Co content in the metalated MOF was determined to be 0.7 Co per Ti_8 node by inductively coupled plasma-mass spectrometry (ICP-MS). Transmission electron microscopy (TEM) imaging showed that Ti_8-BDC-CoCl particles perfectly maintained the plate-like morphology of Ti_8-BDC (Figure 2b and Figure S1, SI). The porosity of Ti_8-BDC-CoCl was evaluated by nitrogen sorption isotherms to afford a Brunauer-Emmett-Teller (BET) surface area of 1479 m^2/g, comparable to that of Ti_8-BDC (1552 m^2/g, Figure 2c).

The Co coordination environment of Ti_8-BDC-CoCl was first optimized by density functional theory (DFT) calculation using the Perdew–Burke–Ernzerhof (PBE) functional.[27-28] DFT optimization converged at a geometry with the octahedral cobalt ion sitting in the Ti_8 octagonal plane and coordinating to two anionic bridging-oxo (μ_2-O^-) groups in the axial positions and two neutral bridging-oxo (μ_2-O) groups in the equa-

torial positions. The Ti_8 node thus acts as a tetradentate oxo-based ligand to form the $[(\mu_2\text{-O})_2(\mu_2\text{-O}^-)_2\text{CoCl(THF)}]^-$ species. The average calculated Co-(μ_2-O$^-$) distance and Co-(μ_2-O) distance were 2.05 Å and 2.27 Å, respectively, consistent with the general trend of shorter M-O distances formed by the anionic oxo ligand than the neutral oxo ligand. The calculated structural model fitted well to the extended X-ray fine structure (EXAFS) data of Co in Ti_8-BDC-CoCl, with average experimental Co-(μ_2-O$^-$) distance and Co-(μ_2-O$^-$) distance of 2.03 Å and 2.25 Å, respectively (Figure 3a). These Co-(OTi) bond distances are also consistent with those reported in the literature.[29]

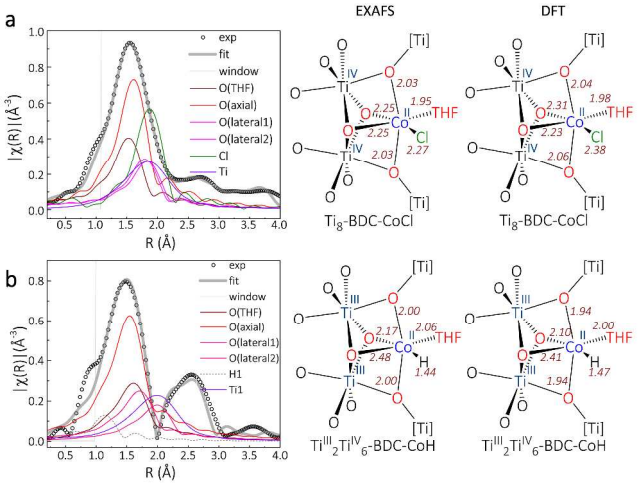

Figure 3. EXAFS spectra (gray circles) and fits (black solid line) in R-space at the Co K-edge adsorption of Ti_8-BDC-CoCl (a) and Ti_8-BDC-CoH (b). The scattering paths of Co to THF-oxygen (wine), axial oxo (red), equatorial oxo (pink), chloride (green), hydride (gray) and titanium (purple) are shown in dashed lines. The EXAFS fitting results agree well with DFT calculated bond distances.

Structure and Electronic Properties of $Ti^{III}_2Ti^{IV}_6$-BDC-Co^{II}H. Upon treatment with $NaBEt_3H$, the color of Ti_8-BDC-CoCl immediately changed from turquoise to navy and then to black with concomitant vigorous evolution of H_2, suggesting Co-mediated electron transfer from the hydride to the Co-Ti_8 system via reductive elimination of H_2 (Figure 4a). Electron paramagnetic resonance (EPR), X-ray photoelectron spectroscopy (XPS), and X-ray absorption near-edge spectroscopy (XANES) were employed to determine whether the reduction occurred at the Co centers or at the Ti centers. The EPR spectra of the reduced sample in toluene clearly displayed two sets of intense signals (Figure 4b). The first sharp isotropic signal, with a g-value of 1.94, is in agreement with those of Ti^{III} species reported in the literature.[30-32] The second set of broad signals, with an average g-value of 2.32, is consistent with those of high-spin d^7 Co^{II} species reported in the literature.[33] Co 2p XPS data of the reduced MOF displayed strong $2p_{3/2}$ and $2p_{1/2}$ peaks at 781.4 eV and 797.4 eV along with strong $2p_{3/2}$ and $2p_{1/2}$ shake-up peaks at 786.8 eV and 803.4 eV, which are characteristic of a high-spin Co^{II} species (Figure 4c).[33] We thus inferred that the reduction occurred at the Ti centers and formulated the reduced Co-Ti_8 system as $Ti^{III}_2Ti^{IV}_6$-BDC-Co^{II}H. High-spin Co^{II} centers indicate the weak field nature of the oxo ligands, which is different from those of the widely investigated C-, N-, or P-based pincer ligands.[34-35] Such oxo-based ligands are difficult to access in molecular systems due to their tendency to bridge multiple metal centers. Co K-edge XANES spectra of Ti_8-BDC-CoCl, $Ti^{III}_2Ti^{IV}_6$-BDC-CoH, and Ti^{IV}_8-BDC-CoH were compared against $CoCl_2$, where the pre-edge of the three MOFs aligned well to that of $CoCl_2$, indicating Co^{II} centers in all three MOFs (Figure 4d). EPR, XPS, and XANES results thus indicated that the Ti^{IV} centers, not the Co^{II} centers, were reduced during the treatment of Ti_8-BDC-CoCl with $NaBEt_3H$.

To quantify the amount of Ti^{III} species per Ti_8 cluster, the reduced MOF was titrated with ferrocenium hexafluorophosphate ($FcPF_6$, 1 mM in CH_2Cl_2).[36] Gas chromatography (GC) quantification indicated the formation of 2.07±0.11 equiv. of ferrocene with respect to Co. The Co centers in the oxidized MOF maintained Co^{II} oxidation state as indicated by K-edge XANES analysis (Figure 4d). Also, hydrides attached to Co^{II} centers are generally known to be poorly reducing through electron transfer reactions.[37] We thus conclude that the Fc^+ oxidation reaction only occurs at Ti^{III} centers, suggesting a $Ti^{III}_2Ti^{IV}_6$ composition of the Co-metalated Ti_8 node (Figure 5a). EXAFS fitting revealed that the Co coordination environment in the MOF after ferrocenium oxidation, Ti^{IV}_8-BTC-CoH, was similar to that in $Ti^{III}_2Ti^{IV}_6$-BDC-CoH (Figure 5b). Thus Ti^{IV}_8-BTC-CoH was used as a control for both spectroscopic analyses and catalytic reactions in subsequent studies. The partial reduction of Ti^{IV} to Ti^{III} was also evidenced by XPS and XANES analysis. The Ti^{IV}_8 node in Ti_8-BDC displayed $2p_{3/2}$ and $2p_{1/2}$ peaks at 458.8 eV and 464.6 eV, respectively, which provided the benchmark for Ti 2p XPS analysis. The Ti $2p_{3/2}$ and $2p_{1/2}$ binding energies for $Ti^{III}_2Ti^{IV}_6$-BDC-CoH shifted lower to 458.4 eV and 464.3 eV, respectively, consistent with partial reduction of Ti^{IV} centers (Figure 4f). Fitting of the $2p_{3/2}$ peak with Ti^{III} and Ti^{IV} components converged at 1:3 ratio, with binding energy of 458.0 eV and 458.5 eV, respectively. The two weak signals at 461.2 eV and 466.9 eV are likely Ti^{III} shake-up satellites, which are characteristic of Ti^{III} centers with unpaired d electrons.[38-39]

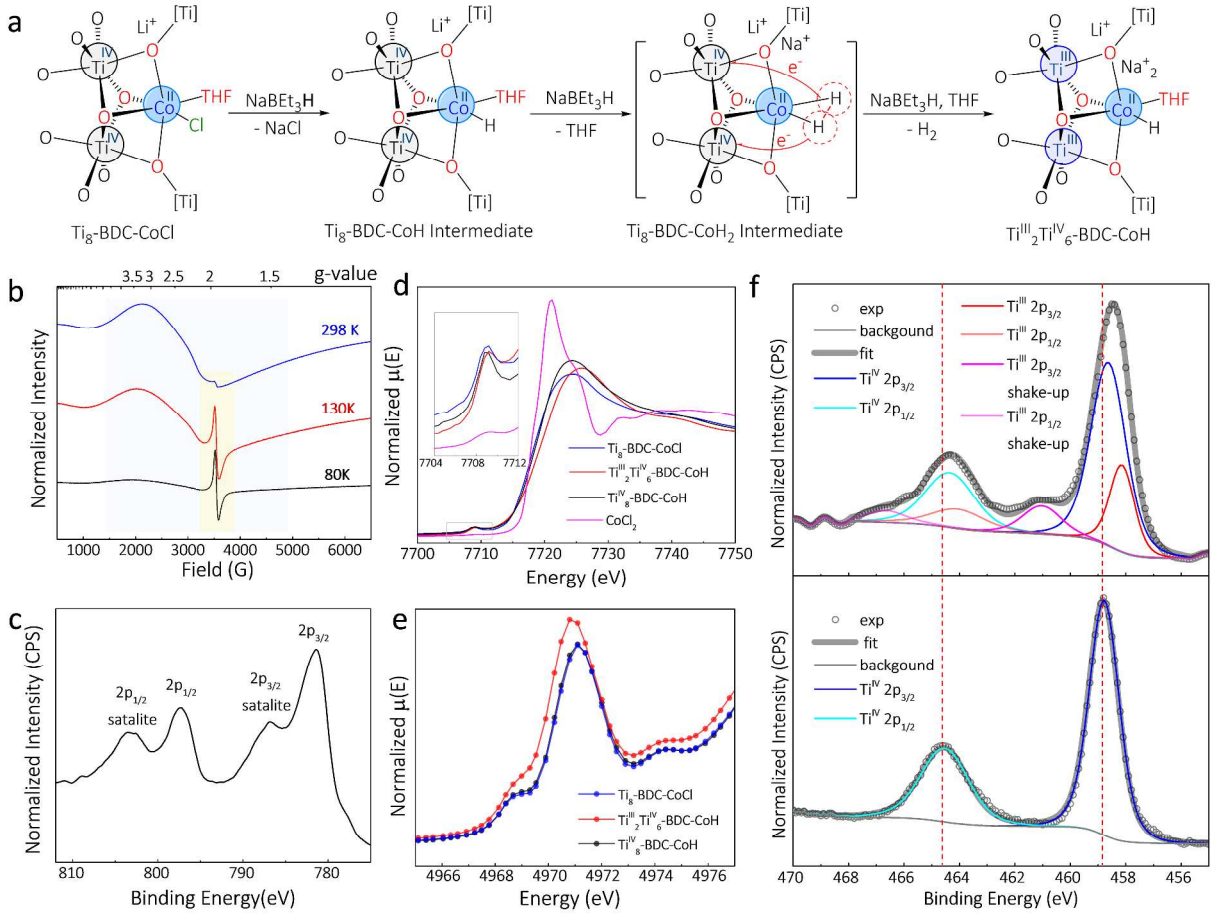

Figure 4. (a) Proposed reduction of Ti_8-BDC-CoCl to $Ti^{III}{}_2Ti^{IV}{}_6$-BDC-CoH with $NaBEt_3H$ via electron spillover from Co to Ti through reductive elimination of H_2. (b) EPR spectra of $Ti^{III}{}_2Ti^{IV}{}_6$-BDC-CoH at 80 K (black), 130 K (red), and 293 K (blue). The signal from Ti^{III} is shaded in yellow, and the signals from Co^{II} are shaded in blue. (c) Co 2p XPS spectra of $Ti^{III}{}_2Ti^{IV}{}_6$-BDC-CoH displayed 4 peaks at 781.4 eV ($2p_{3/2}$), 786.8 eV ($2p_{3/2}$ shake-up), 797.4 eV ($2p_{1/2}$) and 803.4 eV ($2p_{1/2}$ shake-up). (d) Co K-edge XANES spectra of Ti_8-BDC-CoCl (blue), $Ti^{III}{}_2Ti^{IV}{}_6$-BDC-CoH (red) and $Ti^{IV}{}_8$-BDC-CoH (black) compared against $CoCl_2$ (magenta). The pre-edge of the three MOFs aligned well to that of $CoCl_2$, showing Co^{II} centers in all three MOFs. (e) XANES analysis of $Ti^{IV}{}_8$-BDC-CoCl (blue), $Ti^{III}{}_2Ti^{IV}{}_6$-BDC-CoH (red), and $Ti^{IV}{}_8$-BDC-CoH (black) at the Ti K-edge pre-edge region. (f) Ti 2p XPS spectra of $Ti^{IV}{}_8$-BDC (bottom) and $Ti^{III}{}_2Ti^{IV}{}_6$-BDC-CoH (top). The experimental data (gray circles) fit well (gray bold line) with a 3:1 ratio of Ti^{IV} and Ti^{III} species.

The XANES pre-edge region of $Ti^{III}{}_2Ti^{IV}{}_6$-BDC-CoH showed an overall 0.3 eV shift to lower energy compared to that of $Ti^{IV}{}_8$-BDC-CoCl, due to the presence of Ti^{III} centers which enables the lower energy $1s \rightarrow 3d^1$ transition in addition to the $1s \rightarrow 3d^0$ transition (Figure 4e).[39] Furthermore, the pre-edge region of Ti_8-BDC-CoH has higher overall intensity than that of the Ti_8-BDC-CoCl, presumably due to geometry distortion of $[TiO_6]^{3-}$ or $[TiO_6]^{2-}$ octahedra caused by partial reduction, which leads to higher probability of spin-forbidden 1s to 3d transition.[40] In contrast, $Ti^{IV}{}_8$-BTC-CoH displays identical pre-edge signals as Ti_8-BDC-CoCl, supporting the assignment of the aforementioned features to a change in the Ti oxidation state.

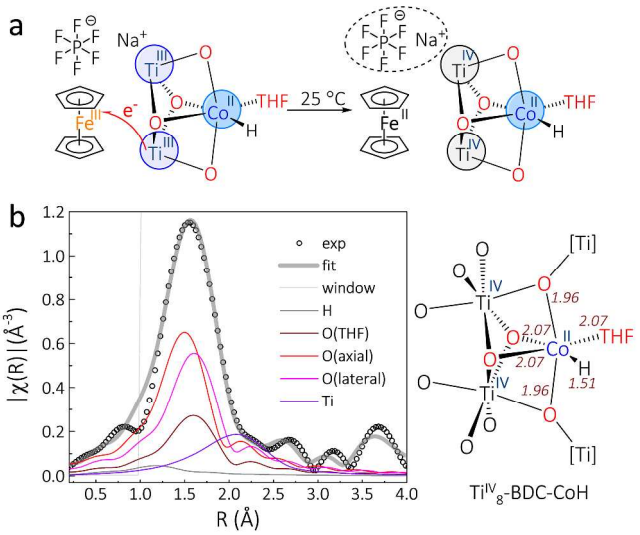

Figure 5. (a) Oxidation of Ti^{III} to Ti^{IV} with $FcPF_6$ through an electron transfer reaction. (b) EXAFS spectrum (gray circles) and

fit (black solid line) in R-space at the Co K-edge adsorption of Ti^{IV}_8-BDC-CoH. The scattering paths of Co to THF-oxygen (wine), axial oxo (red), equatorial oxo (pink), hydride (gray), and titanium (purple) are shown in dashed lines.

The Co coordination environment and electronic structure in $Ti^{III}_2Ti^{IV}_6$-BDC-CoH were studied through DFT calculation using the PBE functional. The Co center in $Ti^{III}_2Ti^{IV}_6$-BDC-CoH maintained a similar coordination geometry to that in Ti_8-BDC-CoCl, with average calculated Co-(μ_2-O^-) distance and Co-(μ_2-O) distance of 1.94 Å and 2.10/2.41 Å, respectively. The calculated structural model was used to fit the Co K-edge EXAFS data, affording an experimental Co-(μ_2-O^-) distance and Co-(μ_2-O^-) distance of 2.00 Å and 2.17/2.48 Å, respectively. The DFT structure of Co^{II} centers thus agreed well with that of EXAFS fitting (Figure 3b).

Table 1 | Optimization of $Ti^{III}_2Ti^{IV}_6$-BDC-CoH Catalyzed Arene Hydrogenation[a]

Entry	Reaction	Catalyst (mol % Loading)	T (°C)	Time (h)	Yield	TON	TOF (h^{-1})
1	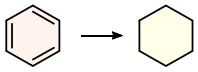	$Ti^{III}_2Ti^{IV}_6$-BDC-CoH (0.05 %)	120	1.5	100 %	≥2000	1333
2[b]		$Ti^{III}_2Ti^{IV}_6$-BDC-CoH (0.005 %)	140	1.5	53 %	10526	7017
3		$Ti^{III}_2Ti^{IV}_6$-BDC-CoH (0.05 %)	80	18	100 %	≥2000	111
4		$Ti^{III}_2Ti^{IV}_6$-BDC-CoH (0.2 %)	25	18	66 %	330	18
5	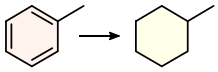	$Ti^{III}_2Ti^{IV}_6$-BDC-CoH (0.005 %)	160	1.5	42 %	8400	5600
6		$Ti^{III}_2Ti^{IV}_6$-BDC-CoH (0.05 %)	120	1.5	76 %	1520	1013
7		Ti^{IV}_8-BDC-CoH (0.05 %)	120	1.5	0 %	0	0

[a]Reaction conditions: Parr high pressure reactor, freshly prepared $Ti^{III}_2Ti^{IV}_6$-BDC-CoH, neat arene substrate, 50 bar H_2 unless specified. [b]120 bar H_2.

$Ti^{III}_2Ti^{IV}_6$-BDC-Co^{II}H Catalyzed Arene Hydrogenation. Arene hydrogenation is of great importance to the industrial production of commodity and fine chemicals, such as cyclohexane analogues, polyester monomers, and plasticizers. With increasingly stringent environmental and health regulations over carcinogenic aromatic compounds,[41] dearomatization reactions, notably arene hydrogenations, are playing a bigger role in diesel fuel refining/upgrading[42] and polymer productions.[43] Conventional arene hydrogenation catalysts include Ni, Ru, Pd, and Pt nanoparticles supported on metal oxides or carbon materials.[44] However, the exact structures and reaction mechanisms of these catalysts remain elusive due to the presence of multiple catalytic species and involvement of multimetallic catalytic pathways.[45]

Although many small-molecule coordination complexes were reported as homogeneous arene hydrogenation catalysts, most of them have been shown to be precursors to nanoparticle catalysts, evidenced by their long induction periods, short life times, and mercury deactivation.[46] Arenes are difficult to hydrogenate with a single metal center, due to their inertness and relatively weak coordination to metal centers. To date, there are few examples of single-site arene hydrogenation catalysts based on late transition metals[47] or early transition metals.[48-49] $Ti^{III}_2Ti^{IV}_6$-BDC-CoH is a MOF-based single-site solid catalyst which cannot undergo a bimetallic decomposition due to active site isolation, representing a unique platform to study non-nanoparticle catalyzed arene hydrogenations.

Benzene and toluene were chosen as model compounds to optimize hydrogenation reaction conditions. At 120 °C under 50 bar H_2, only 0.05 mol% loading of the $Ti^{III}_2Ti^{IV}_6$-BDC-CoH catalyst (based on Co) was needed to completely hydrogenate benzene to produce cyclohexane in 100% yield in 1.5 h, affording a turnover frequency (TOF) of 1333 h^{-1} (Table 1, entry 1). At 140 °C and 120 bar H_2, an impressive TOF of 7017 h^{-1} was obtained with a catalyst loading of 0.005 mol% (Table 1, entry 2). To our knowledge, this is one of the highest TOFs reported for a benzene hydrogenation catalyst, assuming every supported metal to be catalytically active.[50] Exceptionally high TOFs were also obtained with substituted arenes. At 160 °C and 50 bar H_2, toluene was hydrogenated to methylcyclohexane in 42% yield in 1.5 h, with a TOF of 5600 h^{-1} (Table 1, entry 5). $Ti^{III}_2Ti^{IV}_6$-BDC-CoH also exhibited high activity at room temperature, hydrogenating benzene to cyclohexane in 66 % yield at 0.2 mol% of catalyst loading (Table 1, entry 4). $Ti^{III}_2Ti^{IV}_6$-BDC-CoH was reused for at least 6 times for benzene hydrogenation without a decrease in yields, highlighting the robustness and recyclability of this catalyst (Figure S15, SI). Mercury test of $Ti^{III}_2Ti^{IV}_6$-BDC-CoH catalyzed benzene hydrogenation ruled out the involvement of Co nanoparticles (Figure S16, SI). High thermal stability of $Ti^{III}_2Ti^{IV}_6$-BDC-CoH is particularly interesting in terms of potential industrial application considering the exothermic nature of arene hydrogenation reactions.

Table 2 | $Ti^{III}_2Ti^{IV}_6$-BDC-CoH Catalyzed Arene Hydrogenation[a]

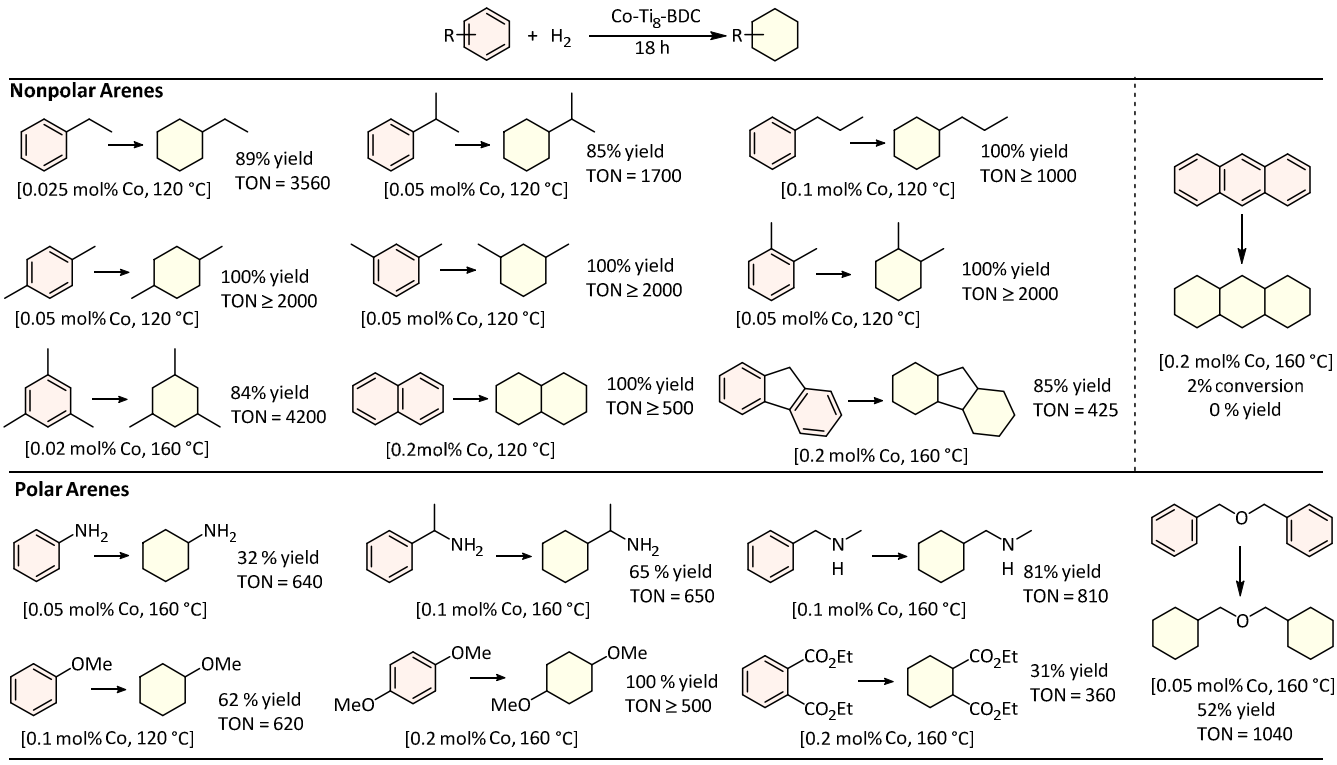

[a]Reaction conditions: Parr high pressure reactor, freshly prepared $Ti^{III}_2Ti^{IV}_6$-BDC-CoH, neat arene substrate, 50 bar H_2.

To investigate the impact of metal-support interactions on the catalyst performance, Ti^{IV}_8-BDC-CoH, generated by $FcPF_6$ oxidation (see above), was also tested for toluene hydrogenation. At 0.05 mol% catalyst loading and under identical reaction conditions, $Ti^{III}_2Ti^{IV}_6$-BDC-CoH converted toluene to cyclohexane in 76 % yield while Ti^{IV}_8-BDC-CoH displayed no catalytic activity (Table 1, entries 6-7). This experiment indicates that the reduction of Ti^{IV}_8 support to $Ti^{III}_2Ti^{IV}_6$ is crucial for the catalytic activity. $Ti^{III}_2Ti^{IV}_6$ provides a more electron-donating oxo-based ligand to afford electron-rich high-spin Co^{II} centers which enable efficient H_2 cleavage and arene dearomatization. This result offers a molecular level understanding for the role of reduced Ti in the SMSI effect which is often observed in TiO_2-supported catalysts.

$Ti^{III}_2Ti^{IV}_6$-BDC-CoH catalyzed arene hydrogenation exhibited an exceptionally broad substrate scope (Table 2). Monosubstituted benzenes, including toluene, ethylbenzene, cumene, and n-propylbenzene, were readily hydrogenated to corresponding saturated hydrocarbons in almost quantitative yields and high turnover numbers (TONs). Disubstituted benzenes, including *p*-, *m*-, and *o*-xylenes, were quantitatively hydrogenated to corresponding dimethylcyclohexanes with TONs of ≥2000. Mesitylene was hydrogenated to 1,3,5-trimethylcyclohexane in 84% yield at 160 °C. Impressively, at 0.2 mol% catalyst loading, polyarenes, including naphthalene and fluorene, were perhydrogenated in 100% and 85% yields, respectively. One unique feature of MOF catalysts is the size-exclusion effect, originating from the uniform shape and size of MOF channels/cages. In contrast to fluorene, anthracene was perhydrogenated in only 2% conversion under identical reaction conditions. $Ti^{III}_2Ti^{IV}_6$-BDC-CoH is thus potentially useful in industrially relevant size-selective arene hydrogenations.

$Ti^{III}_2Ti^{IV}_6$-BDC-CoH also tolerates a variety of polar substituents on arenes. Arenes with amino groups, including aniline, α-methylbenzylamine, and N-methylbenzylamine, were all hydrogenated in high yields without substrate/product inhibition. Aryl ethers, such as anisole and 1,4-dimethoxybenzene, and benzylic ethers, such as dibenzyl ether, were all hydrogenated to corresponding cyclohexyl ethers in good yields without ether hydrogenolysis. The hydrogenation of dialkyl phthalates and terephthalates to corresponding aliphatic esters models an important industrial process for producing green plasticizers, which cannot be achieved with other reported arene hydrogenation catalysts due to electron deficiency and steric hindrance.[51] $Ti^{III}_2Ti^{IV}_6$-BDC-CoH hydrogenated diethyl phthalate to produce diethyl cyclohexane-1,2-dicarboxylate in 31% yield at 160 °C.

$Ti^{III}_2Ti^{IV}_6$-BDC-Co^{II}H Catalyzed Heteroarene Hydrogenation. Heteroarene hydrogenation is an efficient method to generate saturated heterocycles, which are very common structural motifs in pharmaceuticals and biologically active natural products.[52-53] However, compared to other unsaturated compounds, heteroarenes are generally very difficult to hydrogenate due to aromaticity stabilization and heteroatom inhibition. $Ti^{III}_2Ti^{IV}_6$-BDC-CoH was highly active for the hydrogenation of a variety of heteroarenes (Table 3). At 0.05 mol% loading, $Ti^{III}_2Ti^{IV}_6$-BDC-CoH catalyzed pyridine perhydrogenation to piperidine in 94% yield without forming any ring-cleavage products, making it one of the most active and selective catalysts for pyridine reduction. More hindered pyridines, such as 2,6-lutidine and 2,4,6-collidine, were also hydrogenated in almost quantitative yields to the corresponding piperidines.

Impressively, for the hydrogenation of 2,6-lutidine, the catalyst was recycled 10 times without any decrease in yields (Figure S20, SI), supporting the heterogeneity and robustness of the MOF catalyst. Quinoline derivatives, including 3-methylquinoline and 2,6-dimethylquinoline, were perhydrogenated to the corresponding decahydroquinolines in over 90% yields. For substrates with a strong electron withdrawing group, such as 6-chloroquinoline, hydrogenation occurred only at the non-substituted ring, generating the tetrahydroquinoline product. Other heterocyclic systems, such as indole and benzofuran, were also semi-hydrogenated to indoline and dihydrobenzofuran in good yields.

Table 3 | Ti_8-BDC-CoH Catalyzed Heteroarene Hydrogenation[a]

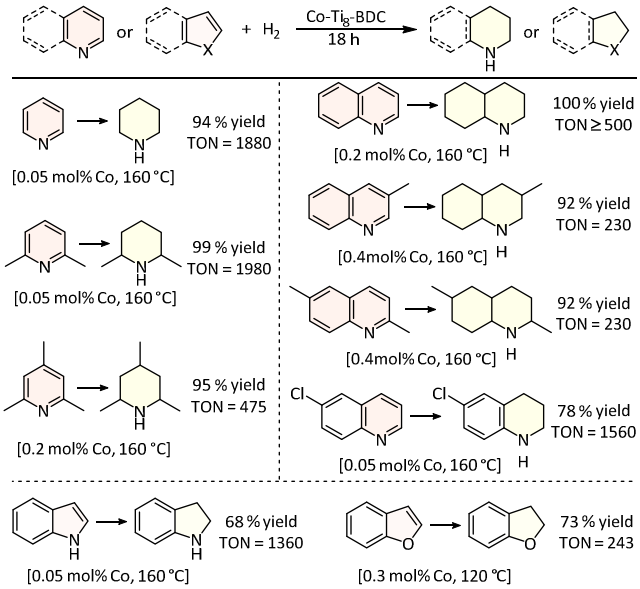

[a]Reaction condition: Parr high pressure reactor, freshly prepared $Ti^{III}_2Ti^{IV}_6$-BDC-CoH, neat heteroarene substrate, 50 bar H_2.

Conclusions

The $Ti_8(\mu_2\text{-}O)_8(\mu_2\text{-}OH)_4$ node of the Ti_8-BDC MOF (MIL-125) was shown to provide an excellent molecular model of TiO_2 to support a single-site Co^{II}-hydride catalyst for arene hydrogenation. Upon deprotonation, the Ti-oxo clusters of Ti_8-BDC coordinated to Co^{II} centers as a tetradentate ligand to afford Ti_8-BDC-CoCl without the complication of forming multi-Co oligomers due to the MOF site isolation effect. Treatment of Ti_8-BDC-CoCl with $NaBEt_3H$ led to partial reduction of the Ti-oxo support via electron spillover from Co to Ti by reductive elimination of H_2 to form $Ti^{III}_2Ti^{IV}_6$-BDC-$Co^{II}H$ whose electronic property was established by EPR, XPS, XANES, DFT, and ferrocenium oxidation. $Ti^{III}_2Ti^{IV}_6$-BDC-$Co^{II}H$ features electron-rich high spin Co^{II} centers with electron-donating Ti^{III}-oxo ligands and is one of few highly active molecular, non-nanoparticle catalysts for arene and heteroarene hydrogenation. Interestingly, the corresponding oxidized MOF Ti^{IV}_8-BDC-$Co^{II}H$ is totally inactive in arene hydrogenation, proving the crucial role of Ti-oxo cluster reduction on the catalytic activity of supported Co^{II}-H species. The Ti_8-BDC MOF thus provides a molecularly precise model of metal oxo clusters for understating the strong metal-support interaction of TiO_2-supported heterogeneous catalysts. The single-site nature of MOF node-supported catalysts should allow detailed spectroscopic and computational investigations, thus promising a deep understanding of key parameters influencing catalytic performances and rational design of effective arene hydrogenation catalysts to meet the ever increasing environmental and health regulations for the chemical industry.

Experimental Methods

Synthesis of Ti_8-BDC-CoCl. In an N_2-filled glovebox, $LiCH_2SiMe_3$ (1.0 M in pentane, 2.3 mL, 10 equiv. to Ti_8 node) was added dropwise to a suspension of Ti_8-BDC (500 mg, 29% solvent content by TGA, 0.23 mmol Ti_8 node) in 15 mL hexanes. After being stirred at 25 °C for 6 h, the resulting light-yellow solid was collected through centrifugation, and washed with hexanes six times. The lithiated Ti_8-BDC was then transferred to a vial containing 11.5 mL of a $CoCl_2$ solution in THF (20 mM). This mixture was stirred for 12 h at 25 °C and the turquoise solid was then centrifuged and washed with THF five times. The Ti_8-BDC-CoCl was freeze-dried in benzene and stored in the glovebox for further use. ICP-MS analysis showed a Ti/Co ratio of 11.4, indicating 0.7 Co per Ti_8 node. PXRD, TEM and BET showed the crystallinity of MOF was maintained after metalation.

Synthesis of $Ti^{III}_2Ti^{IV}_6$-BDC-CoH. In an N_2-filled glove box, Ti_8-BDC-CoCl (10.0 μmol of Co) was charged to a 1.5 mL centrifuge tube and dispersed in 1.0 mL of toluene. $NaBEt_3H$ (0.1 mL, 0.1 mmol, 1.0 M solution in toluene) was then added dropwise to the suspension. The color of the MOF changed immediately from turquoise to deep blue and then to black while vigorously evolving H_2 gas. The resulting suspension was kept at r.t. for 30 min to ensure complete reduction. The black solid was then centrifuged out of suspension and washed three times with toluene to remove excess $NaBEt_3H$ and other byproducts (NaCl and BEt_3).

Oxidation of $Ti^{III}_2Ti^{IV}_6$-BDC-CoH to Ti^{IV}_8-BDC-CoH. A ferrocenium hexafluorophosphate ($FcPF_6$) solution (1 mM in CH_2Cl_2) was added to $Ti^{III}_2Ti^{IV}_6$-BDC-CoH (10 μmol of Co) in 3 mL aliquots. Upon this addition, the suspension was vortexed and its immediately changed from deep blue to yellow, indicating rapid reduction of ferrocenium to ferrocene by Ti^{III}. The suspension was then centrifuged and the yellow supernatant was combined in a separate vial. This reduction process was repeated until no color change (from deep blue to yellow) could be observed within 10 min. Upon completion, 8 equiv. of mesitylene w.r.t. Co were added to the combined supernatant as an internal standard, and the amount of ferrocene was analyzed by GC.

A typical procedure for $Ti^{III}_2Ti^{IV}_6$-BDC-CoH catalyzed hydrogenation of arenes and heteroarenes. In an N_2-filled glove box, Ti_8-BDC-CoCl (5 μmol of Co) in 1.0 mL heptane was charged into a glass vial. $NaBEt_3H$ (10 equiv. to Co, 50 μL, 1.0 M in toluene) was then added to the vial and the mixture was stirred for 30 min. The solid was then centrifuged, washed with heptane three times, and transferred to a Parr reactor with a glass liner using benzene (0.89 mL, 10 mmol). The reactor was sealed in the glovebox, and then charged with hydrogen to 50 bar. After stirring at 120 °C for 18 h, the pres-

sure was released and the MOF catalyst was removed from the reaction mixture via centrifugation. The supernatant was then analyzed by ^{1}H NMR, revealing a 100% yield of cyclohexane. ICP-MS analysis of the supernatant showed <0.1% leaching of Co from the $Ti^{III}_2Ti^{IV}_6$-BDC-CoH catalyst.

ASSOCIATED CONTENT

Supporting Information. Synthesis and characterization of Ti_8-BDC-CoCl, $Ti^{III}_2Ti^{IV}_6$-BDC-CoH, Ti^{IV}_8-BDC-CoH; Reaction procedures and product characterizations for catalytic hydrogenation of arenes and heteroarenes; This material is available free of charge via the Internet at http://pubs.acs.org.

AUTHOR INFORMATION

Corresponding Author

*wenbinlin@uchicago.edu
*xdp@imm.ac.cn

Author Contributions

The manuscript was written through contributions of all authors. All authors have given approval to the final version of the manuscript.

Notes

The authors declare no competing financial interest.

ACKNOWLEDGMENT

This work was supported by National Science Foundation (CHE-1464941). X-ray absorption spectroscopy analysis was performed at Beamline 9-BM, supported by the Materials Research Collaborative Access Team (MRCAT). Use of the Advanced Photon Source, an Office of Science User Facility operated for the U.S. DOE Office of Science by ANL, was supported by the U.S. DOE under Contract No. DE-AC02-06CH11357. We thank Guangxu Lan for help with TEM and Dr. Alexander S. Filatov for help with XPS.

REFERENCES

References

1. Bourikas, K.; Kordulis, C.; Lycourghiotis, A., *Chem. Rev.* **2014,** *114*, 9754-9823.
2. Siddiqi, G.; Mougel, V.; Copéret, C., *Inorg. Chem.* **2016,** *55*, 4026-4033.
3. Matsubu, J. C.; Zhang, S.; DeRita, L.; Marinkovic, N. S.; Chen, J. G.; Graham, G. W.; Pan, X.; Christopher, P., *Nat Chem* **2017,** *9*, 120-127.
4. Tauster, S., *Acc. Chem. Res.* **1987,** *20*, 389-394.
5. Park, J. Y.; Baker, L. R.; Somorjai, G. A., *Chem. Rev.* **2015,** *115*, 2781-2817.
6. Dulub, O.; Hebenstreit, W.; Diebold, U., *Phys. Rev. Lett.* **2000,** *84*, 3646-3649.
7. Chen, M. S.; Goodman, D. W., *Science* **2004,** *306*, 252-255.
8. Baker, L. R.; Kennedy, G.; Van Spronsen, M.; Hervier, A.; Cai, X.; Chen, S.; Wang, L.-W.; Somorjai, G. A., *J. Am. Chem. Soc.* **2012,** *134*, 14208-14216.
9. Shi, F.; Baker, L. R.; Hervier, A.; Somorjai, G. A.; Komvopoulos, K., *Nano Lett.* **2013,** *13*, 4469-4474.
10. Lazzeri, M.; Selloni, A., *Phys. Rev. Lett.* **2001,** *87*, 266105.
11. Yang, H. G.; Sun, C. H.; Qiao, S. Z.; Zou, J.; Liu, G.; Smith, S. C.; Cheng, H. M.; Lu, G. Q., *Nature* **2008,** *453*, 638-641.
12. Morgan, B. J.; Watson, G. W., *The J. Phys. Chem. C* **2009,** *113*, 7322-7328.
13. Ma, L.; Abney, C.; Lin, W., *Chem. Soc. Rev.* **2009,** *38*, 1248-1256.
14. Lee, J.; Farha, O. K.; Roberts, J.; Scheidt, K. A.; Nguyen, S. T.; Hupp, J. T., *Chem. Soc. Rev.* **2009,** *38*, 1450-1459.
15. Yoon, M.; Srirambalaji, R.; Kim, K., *Chem. Rev.* **2012,** *112*, 1196-1231.
16. Davis, M. E., *Nature* **2002,** *417*, 813.
17. Na, K.; Choi, K. M.; Yaghi, O. M.; Somorjai, G. A., *Nano Lett.* **2014,** *14*, 5979-5983.
18. Ikuno, T.; Zheng, J.; Vjunov, A.; Sanchez-Sanchez, M.; Ortuño, M. A.; Pahls, D. R.; Fulton, J. L.; Camaioni, D. M.; Li, Z.; Ray, D.; Mehdi, B. L.; Browning, N. D.; Farha, O. K.; Hupp, J. T.; Cramer, C. J.; Gagliardi, L.; Lercher, J. A., *J. Am. Chem. Soc.* **2017,** *139*, 10294-10301.
19. Zhang, Z.-M.; Zhang, T.; Wang, C.; Lin, Z.; Long, L.-S.; Lin, W., *J. Am. Chem. Soc.* **2015,** *137*, 3197-3200.
20. Ma, L.; Falkowski, J. M.; Abney, C.; Lin, W., *Nat. Chem.* **2010,** *2*, 838-846.
21. Manna, K.; Ji, P.; Lin, Z.; Greene, F. X.; Urban, A.; Thacker, N. C.; Lin, W., **2016,** *7*, 12610.
22. Ji, P.; Sawano, T.; Lin, Z.; Urban, A.; Boures, D.; Lin, W., *J. Am. Chem. Soc.* **2016,** *138*, 14860-14863.
23. Xiao, D. J.; Bloch, E. D.; Mason, J. A.; Queen, W. L.; Hudson, M. R.; Planas, N.; Borycz, J.; Dzubak, A. L.; Verma, P.; Lee, K.; Bonino, F.; Crocellà, V.; Yano, J.; Bordiga, S.; Truhlar, D. G.; Gagliardi, L.; Brown, C. M.; Long, J. R., *Nat Chem* **2014,** *6*, 590-595.
24. Comito, R. J.; Fritzsching, K. J.; Sundell, B. J.; Schmidt-Rohr, K.; Dincă, M., *J. Am. Chem. Soc.* **2016,** *138*, 10232-10237.
25. Dan-Hardi, M.; Serre, C.; Frot, T.; Rozes, L.; Maurin, G.; Sanchez, C.; Férey, G., *J. Am. Chem. Soc.* **2009,** *131*, 10857-10859.
26. Conner Jr, W. C.; Falconer, J. L., *Chem. Rev.* **1995,** *95*, 759-788.
27. Frisch, M.; Trucks, G.; Schlegel, H.; Scuseria, G.; Robb, M.; Cheeseman, J.; Zakrzewski, V.; Montgomery Jr, J.; Stratmann, R.; Burant, J., Gaussian 09, Gaussian, Inc., Pittsburgh, PA, 2009;.
28. Perdew, J. P.; Burke, K.; Ernzerhof, M., *Phys. Rev. Lett.* **1996,** *77*, 3865.
29. Lei, X.; Shang, M.; Fehlner, T. P., *Organometallics* **1997,** *16*, 5289-5301.
30. Mason, J. A.; Darago, L. E.; Lukens Jr, W. W.; Long, J. R., *Inorg. Chem.* **2015,** *54*, 10096-10104.
31. Entley, W. R.; Treadway, C. R.; Wilson, S. R.; Girolami, G. S., *J. Am. Chem. Soc.* **1997,** *119*, 6251-6258.
32. Spannenberg, A.; Tillack, A.; Arndt, P.; Kirmse, R.; Kempe, R., *Polyhedron* **1998,** *17*, 845-850.
33. Léonard, N. G.; Bezdek, M. t. J.; Chirik, P. J., *Organometallics* **2016,** *36*, 142-150.
34. Léonard, N. G.; Bezdek, M. J.; Chirik, P. J., *Organometallics* **2017,** *36*, 142-150.

35. Bowman, A. C.; Milsmann, C.; Bill, E.; Lobkovsky, E.; Weyhermüller, T.; Wieghardt, K.; Chirik, P. J., *Inorg. Chem.* **2010,** *49*, 6110-6123.
36. Scherer, A.; Haase, D.; Saak, W.; Beckhaus, R. d.; Meetsma, A.; Bouwkamp, M. W., *Organometallics* **2009,** *28*, 6969-6974.
37. Ciancanelli, R.; Noll, B. C.; DuBois, D. L.; DuBois, M. R., *J. Am. Chem. Soc.* **2002,** *124*, 2984-2992.
38. Milošv, I.; Strehblow, H. H.; Navinšek, B.; Metikoš Huković, M., *Surf. Interface Anal.* **1995,** *23*, 529-539.
39. Durmeyer, O.; Kappler, J.; Beaurepaire, E.; Heintz, J.; Drillon, M., *J. Phys.: Condens. Matter* **1990,** *2*, 6127.
40. WlvcnuNls, G. A., *Am. Mineral.* **1987,** *72*, 89-101.
41. Harvey, R. G., Environmental Chemistry of PAHs. In *PAHs and Related Compounds: Chemistry*, Neilson, A. H., Ed. Springer Berlin Heidelberg: Berlin, Heidelberg, 1998; pp 1-54.
42. Corma, A.; Martınez, A.; Martınez-Soria, V., *J. Catal.* **1997,** *169*, 480-489.
43. Bui, T. T.; Giovanoulis, G.; Cousins, A. P.; Magnér, J.; Cousins, I. T.; de Wit, C. A., *Sci. Total Environ.* **2016,** *541*, 451-467.
44. Cui, X.; Surkus, A.-E.; Junge, K.; Topf, C.; Radnik, J.; Kreyenschulte, C.; Beller, M., *Nat. Commun.* **2016,** *7*.
45. Barbaro, P.; Bianchini, C.; Dal Santo, V.; Meli, A.; Moneti, S.; Psaro, R.; Scaffidi, A.; Sordelli, L.; Vizza, F., *J. Am. Chem. Soc.* **2006,** *128*, 7065-7076.
46. Dyson, P. J., *Dalton Transactions* **2003**, 2964-2974.
47. Bleeke, J.; Muetterties, E., *J. Am. Chem. Soc.* **1981,** *103*, 556-564.
48. Gu, W.; Stalzer, M. M.; Nicholas, C. P.; Bhattacharyya, A.; Motta, A.; Gallagher, J. R.; Zhang, G.; Miller, J. T.; Kobayashi, T.; Pruski, M., *J. Am. Chem. Soc.* **2015,** *137*, 6770-6780.
49. Stalzer, M. M.; Nicholas, C. P.; Bhattacharyya, A.; Motta, A.; Delferro, M.; Marks, T. J., *Angew. Chem.* **2016,** *128*, 5349-5353.
50. Kang, X.; Liu, H.; Hou, M.; Sun, X.; Han, H.; Jiang, T.; Zhang, Z.; Han, B., *Angew. Chem.* **2016,** *128*, 1092-1096.
51. Rasero-Almansa, A. M.; Corma, A.; Iglesias, M.; Sánchez, F., *Green Chem.* **2014,** *16*, 3522-3527.
52. Sridharan, V.; Suryavanshi, P. A.; Menéndez, J. C., *Chem. Rev.* **2011,** *111*, 7157-7259.
53. Vitaku, E.; Smith, D. T.; Njardarson, J. T., *J. Med. Chem.* **2014,** *57*, 10257-10274.

For Table of Contents Only